

# Multicritical quantum sensors driven by symmetry-breaking

Sayan Mondal, Ayan Sahoo, Ujjwal Sen and Debraj Rakshit

Harish-Chandra Research Institute, A CI of Homi Bhabha National Institute, Chhatmag Road, Jhunsī, Prayagraj 211 019, India

Quantum criticality has been demonstrated as a useful quantum resource for parameter estimation. This includes second-order, topological and localization transitions. In all these works reported so far, gap-to-gapless transition at criticality has been identified as the ultimate resource for achieving the quantum enhanced sensing, although there are several important concepts associated with criticality, such as long-range correlation, symmetry breaking. In this work, we analytically demonstrate that symmetry-breaking can drive a quantum enhanced sensing in single- or multiparameter estimation. We show this in the well-known Kitaev model, a lattice version of the 1D  $p$ -wave superconductor, which consists of a pairing term and an onsite potential term. The model is characterized by two critical lines and a multi-critical point at the intersection of these two lines. We show that Heisenberg scaling can be obtained in precision measurement of the superconducting coupling by preparing the system at or near the multicritical point despite the fact that parameter variation follows the critical lines, i.e., without an explicit requirement of gap-to-gapless transition. Quantum enhancement in such situations solely occurs due to a global  $U(1)$  symmetry-breaking by the pairing term. Extending our analysis in the realm of multiparameter estimation we show that it is possible to obtain super-Heisenberg scaling by combining the effects of symmetry-breaking and gapless-to-gapped transition.

## I. INTRODUCTION

The quantum Cramér-Rao bound provides the ultimate limit of precision within which an unknown parameter can be estimated in the quantum systems [1–4]. The uncertainty  $\epsilon_q$  in parameter estimation is related to a very special quantity, quantum Fisher information. The bound suggests that  $\epsilon_q \geq (MF_Q)^{-1}$  for the quantum systems, where  $F_Q$  is the quantum Fisher information (QFI) and  $M$  is the number of repetition of the sensing protocol. Quantum systems might provide a true quantum edge over classical systems when it comes to accurately measuring an unknown variable. This is demonstrated by how the uncertainty scales with the size of the probe. Given  $\epsilon_q \propto L^{-\nu}$ , where  $L$  is the prob size and  $\nu$  is the associate scaling exponent, the classical probes can at-best scale linearly with system size, i.e.,  $\nu = 1$ , which corresponds to the standard quantum limit (SQL). However, it is possible to exploit quantum phenomena, such as quantum correlation or cooperative phenomena, for achieving quantum-enhanced sensitivity, where  $\nu > 1$ . The so-called Heisenberg limit (HL) corresponds to  $\nu = 2$  [5]. Subsequently, quantum sensing [2, 6, 7] has taken the centre stage of quantum technology with several applications, and has been investigated from different points of views [5, 8–12].

The cooperative quantum phenomena, such as quantum phase transitions in quantum many-body (QMB) systems, has turned out to be an extremely useful quantum resource for engineering new types of quantum sensors. Quantum criticality, in its various forms, have been utilized to attain HL limit, or for even realizing beyond HL limits. This includes symmetry-breaking second-order quantum phase transitions [13–34], as well as symmetry-protected quantum phase transitions, such as localization transition [35, 36] and topological phase transition (TPT) [37–42], and non-Hermitian topological systems [43–46]. There are two different key motivations for probing different kinds of quantum criticality - first, it is important to understand the basic ingredients leading to quantum-enhanced sensitivity, e.g. the role of gap closing or symmetry-breaking; secondly, there is a constant quest for identifying experimen-

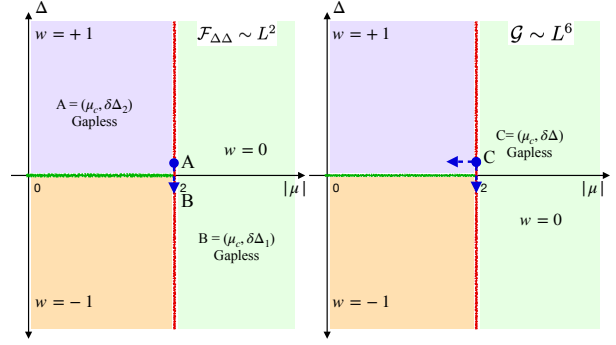


FIG. 1. **Schematic for quantum enhanced sensing assisted by symmetry-breaking:** The phase diagram shows different topological phases in the  $\mu$ - $\Delta$  plane. The red and the green lines are gapless. In the left panel, the protocol of sensing  $\Delta$  is presented.  $\mathcal{F}_{\Delta\Delta}$  has an quantum enhanced scaling when the system is prepared at the critical line of  $\mu = \mu_c$  (near the multicritical point, at A), and driven to, say B. We note that this is enhancement of scaling is not because of gap-to-gapless transition, but rather due to breaking of  $U(1)$  symmetry. In the multi-parameter regime, one can envision a case where system is prepared at C, and both the parameters are maneuvered along the directed arrows. This leads to a quantum enhanced scaling for the multi-parameter precision estimator,  $\mathcal{G} \sim L^6$ . This involves, both, a gap-to-gapless transition and the symmetry-breaking.

tally realizable QMB systems with super-Heisenberg scaling property characterized by large scaling exponent. It has been shown that the gap closing at criticality leads to a scaling of  $F_q \sim L^{(2/\nu)}$ , where  $L$  is the system size, and the critical exponent  $\nu$  characterizing the divergence of the correlation length (localization length) near the criticality in case of the second-order quantum phase transition (localization transition). Although there are many key aspects associated with quantum criticality, such as symmetry breaking, gap closing, long-range correlation, only the gap closing has been identified as the crucial ingredient for obtaining quantum enhanced sensitivity, implying  $\nu < 2$ .

In this work we show that gap-to-gapless transition is always not required for quantum-enhanced sensing. Symmetry-breaking at multi-criticality can also be sufficient for it. In our knowledge such symmetry-breaking quantum advantage for quantum sensing has not been reported in literature previously. We consider well-known Kitaev model on a one-dimensional lattice with nearest neighbor hopping, onsite potential with strength  $\mu$  and a  $p$ -wave pairing term with amplitude  $\Delta$ , for demonstrating the idea analytically. The model has two critical lines at  $\Delta = 0$  and  $|\mu| = 2$ , crossing whom one observes discrete jumps in a topological invariant. It hosts multi-critical points at the intersections of these two critical lines. The system is prepared at or near the multi-critical point. In the context of single parameter estimation we show that precision estimation of  $\Delta$  is still possible, even though then parameter variation in  $\Delta$  is restricted to follow the critical line at  $\mu = 2$ , where it does not encounter any gapless-to-gap transition. We show that the system still can achieve Heisenberg scaling. We expand our interest in the realm of multi-parameter sensing, where we perform simultaneous estimation of both,  $\mu$  and  $\Delta$ . Despite the fact that parameter variations follow the gapless critical lines, super-Heisenberg scaling is observed for multi-parameter estimation. In both the cases the quantum enhanced sensing is essentially facilitated via a symmetry-breaking at  $\Delta = 0$ , at which the system has a  $U(1)$  symmetry. This forms the central result presented in this work.

## II. MODEL

*Model.*— We consider the one-dimensional Kitaev lattice model [47, 48],  $\hat{H} = \hat{H}_1 + \hat{H}_\Delta$ , where

$$\begin{aligned}\hat{H}_1 &= -\sum_{j=1}^L \left( \hat{c}_j^\dagger \hat{c}_{j+1} + h.c. \right) - \mu \sum_{j=1}^L \left( \hat{c}_j^\dagger \hat{c}_j - \frac{1}{2} \right), \\ \hat{H}_\Delta &= \frac{\Delta}{2} \sum_{j=1}^L \left( \hat{c}_j^\dagger \hat{c}_{j+1}^\dagger + h.c. \right).\end{aligned}\quad (1)$$

Here  $\hat{c}_j^\dagger$  ( $\hat{c}_j$ ) is the creation (annihilation) operator at site  $i$  of a spinless fermion,  $L$  is the number of lattice sites,  $\mu$  is an on-site potential and  $\Delta$  is the superconducting  $p$ -wave pairing amplitude. This model has a rich topological phase diagram [49–52], which can be characterized via a topological invariant, the winding number,  $w$ . Two critical lines  $\mu = \pm 2$  and  $\Delta = 0$  set apart three topologically distinct phases: a trivial phase for  $|\mu| > 2$  with  $w = 0$ , one topologically non-trivial phase for  $|\mu| < 2$  with  $w = 1$  for  $\Delta > 0$ , and another topologically non-trivial phase for  $|\mu| < 2$  with  $w = -1$  for  $\Delta < 0$ . The one-dimensional Kitaev model hosts Majorana Zero Modes [53, 54] in the topological phases at both of its ends. The intersections of two critical lines marks two multi-critical points in the system. The multicritical point connects two topologically non-trivial phases with a topologically trivial phase. Topological properties of a  $p$ -wave spin-less superconductor have been studied from different points of views in recent years [51, 55–61]. There has been several proposals

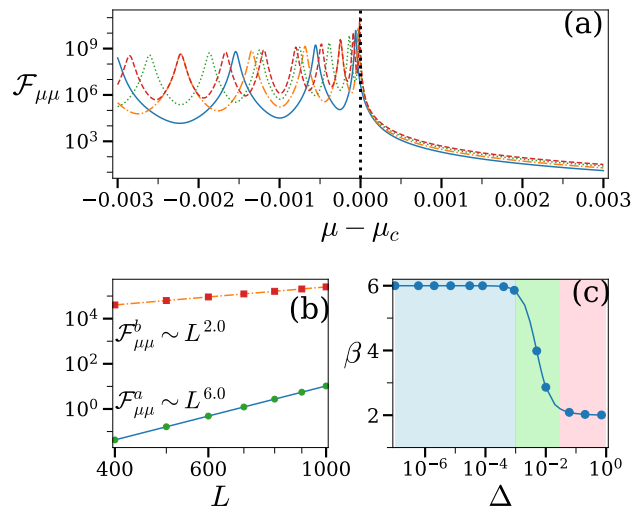


FIG. 2. *The variation of  $\mathcal{F}_{\mu\mu}$  around the multicriticality* : (a)  $\mathcal{F}_{\mu\mu}$  for system sizes  $N = 400$  (solid blue line), 600 (dot-dashed orange line), 800 (dotted green line), 1000 (dashed red line) are presented against  $\mu$ , where in the x-axis  $\mu_c = 2$  has been subtracted from  $\mu$ .  $\Delta = 0.001$  is set for all cases. This is a representative case, we observe a similar nature for various other system-sizes. (b) The finite-size scaling of  $\mathcal{F}_{\mu\mu}$  is presented at  $\mu = 2$  and two different  $\Delta$ . Considering  $\Delta = 10^{-7}$ , we observe  $\mathcal{F}_{\mu\mu}^a \sim L^{6.0}$  (circular markers) and  $\Delta = 0.7$ , we observe  $\mathcal{F}_{\mu\mu}^b \sim L^{2.0}$  (square markers). The straight lines are the best fit. (c) We present the scaling exponents  $\beta$  of  $\mathcal{F}_{\mu\mu}$  against the parameter  $\Delta$ . We identify three regions, (i) low  $\Delta$  regime:  $\Delta < 10^{-3}$  represented by light blue color where  $\mathcal{F}_{\mu\mu} \sim L^6$ ; (ii) intermediate  $\Delta$  regime:  $10^{-3} \leq \Delta \leq 10^{-2}$  is represented by light green color, where  $\mathcal{F}_{\mu\mu} \sim L^\beta$ ,  $\beta \in (2, 6)$ ; (iii) large  $\Delta$  regime:  $\Delta > 10^{-2}$  is represented by light pink color, where  $\mathcal{F}_{\mu\mu} \sim L^2$ . The parameter  $\mu = 2$  is fixed throughout.

and experimental efforts for physical realization of the Kitaev  $p$ -wave model [56, 62–72].

*Many-body ground state.*— The ground state of the Kitaev model under anti-periodic boundary conditions (ABC) is a many-particle state which is given by,

$$|\Psi_G\rangle = \prod_{k=1}^{L/2} (u_k + v_k c_k^\dagger c_{-k}^\dagger) |0\rangle, \quad (2)$$

where  $u_k = (\mathcal{E}_k + z_k)/E_k$  and  $v_k = iy_k/E_k$ . Here  $E_k = \sqrt{2\mathcal{E}_k(\mathcal{E}_k + z_k)}$  with  $\mathcal{E}_k = 2\sqrt{(\cos k + \frac{\mu}{2})^2 + \frac{1}{4}\Delta^2 \sin^2 k}$ ,  $y_k = -\Delta \sin k$  and  $z_k = -\mu - 2 \cos k$ . The ground state is a superposition of states with multiple particle numbers but all are from even parity sector.

## III. MULTI-PARAMETER SENSING

*Essential theory of single- and multi-parameter sensing.*— Recently, sensing for more than one parameter or multi-parameter sensing has gained interest [73–75]. The parameters  $\mu$ ,  $\Delta$  of the Hamiltonian,  $\hat{H}$ , are encoded in the ground state. These parameters are changed, which gets reflected in

the ground state. By employing the methods of the quantum Fisher information matrix (QFIM), we get a  $2 \times 2$  matrix  $\mathcal{F}$  given by  $\mathcal{F}_{ab} = 4\text{Re}(\langle \partial_a \Psi | \partial_b \Psi \rangle - \langle \partial_a \Psi | \Psi \rangle \langle \Psi | \partial_b \Psi \rangle)$ , where  $a, b = \mu, \Delta$  and  $|\Psi\rangle$  is the probe state. While considering multi-parameter sensing, the equally weighted uncertainty is given by,

$$\delta\mu^2 + \delta\Delta^2 \geq \frac{1}{m} \mathcal{G}^{-1}, \quad (3)$$

where  $\mathcal{G} := (\text{Tr}[\mathcal{F}^{-1}])^{-1} = \frac{\mathcal{F}_{\mu\mu}\mathcal{F}_{\Delta\Delta} - \mathcal{F}_{\Delta\mu}\mathcal{F}_{\mu\Delta}}{\mathcal{F}_{\mu\mu} + \mathcal{F}_{\Delta\Delta}}$  and  $m$  is the number of repetition of the sensing protocol. The quantity  $\mathcal{G}^{-1}$  is the total uncertainty for the equally weighted multi-parameter estimation. For the single-parameter estimation case, i.e., when one of the two parameters is precisely known, it is sufficient to compute the relevant diagonal element of the QFIM. Further discussion on this is presented in Appendix A.

*Symmetry-breaking assisted parameter estimation at multicriticality.*— In absence of the pairing term, i.e., for  $\Delta = 0$ , the system has the global  $U(1)$  symmetry as the Hamiltonian is invariant under the transformation  $\hat{c}_i \rightarrow e^{i\phi} \hat{c}_i$ , where  $\phi$  is a site-independent phase. This global symmetry implies the conservation of the total fermion number. The corresponding system is gapless for parameter regime  $|\mu| \leq 2$ . Introduction of  $\hat{H}_\Delta$  breaks the  $U(1)$  symmetry, and a gap opening is occurred. The phase diagram is gaped everywhere in the  $\mu - \Delta$  plane except at the critical lines at  $|\mu| = 2$ . The basic idea of the symmetry-breaking quantum enhancement of precision is the following: For parameter estimation of  $\Delta$ , assuming  $\mu$  as a known parameter that can be precisely tuned, the many-body ground state of the system is prepared near the multi-critical point ( $\mu = 2$  and  $\Delta \rightarrow 0$ ). If the system is subjected to a small variation in  $\Delta$ , it is bound to happen along the gapless critical line at  $\mu = 2$ . As we show below, this gives rise to Heisenberg scaling in  $\mathcal{F}_{\Delta\Delta}$  – thanks to the  $U(1)$  symmetry-breaking. This is not the case with the parameter estimation of  $\mathcal{F}_{\mu\mu}$ . It vanishes on the gapless critical line, and must involve a gap-to-gapless transition by setting  $\Delta$  non-zero. Details related to this will be furnished later. The idea, however, can be generalized for simultaneous estimation of two-parameters by combing the effects of, both, symmetry-breaking and a gap-to-gapless transition. A super-Heisenberg scaling is obtained under such scenario in  $\mathcal{G}$ . The is the main idea that we pitch in this work and is schematically presented in Fig. 1. In the following we present the results.

*QFIM near criticality: Leading-order scaling.*— We begin with summarizing the key results before we proceed to provide further details. We use fidelity based definition of  $\mathcal{F}_{ab}$  for deriving the elements of QFIM for the ground state  $|\Phi_G\rangle$  (Eq. (2)). Following expressions are obtained:  $\mathcal{F}_{\mu\mu} = \sum_k \frac{\Delta^2 \sin^2 k}{\mathcal{E}_k^4}$ ,  $\mathcal{F}_{\mu\Delta} = \sum_k \frac{\Delta z_k \sin^2 k}{\mathcal{E}_k^4}$  and  $\mathcal{F}_{\Delta\Delta} = \sum_k \frac{z_k^2 \sin^2 k}{\mathcal{E}_k^4}$ . Unlike classical Fisher Information, which is additive, Quantum Fisher Information is super-additive. Hence, what are of prime interests are the system-size scalings of the elements of QFIM and the ultimate precision estimator  $\mathcal{G}$ . By calculating the limits of  $\mathcal{F}_{\mu\mu}$  as  $\Delta \rightarrow 0$  and  $\mu \rightarrow 2$ , we

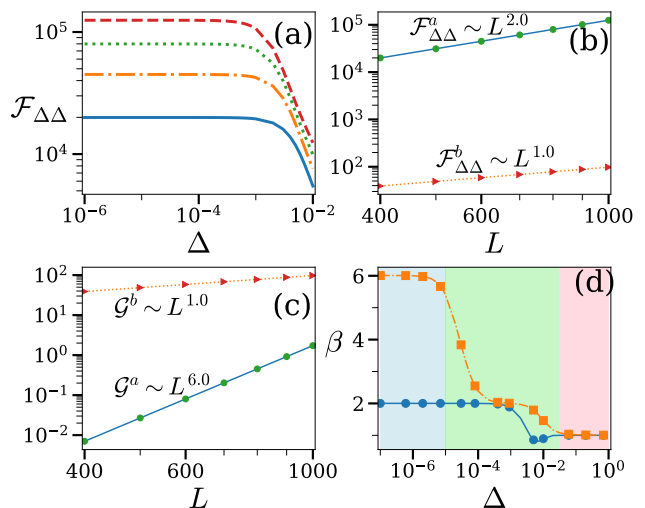


FIG. 3. **Variation of  $\mathcal{F}_{\Delta\Delta}$  and  $\mathcal{G}$  near the multicritical point:** (a)  $\mathcal{F}_{\Delta\Delta}$  for system sizes  $L = 400$  (solid blue line),  $600$  (dot-dashed orange line),  $800$  (dotted green line),  $1000$  (dashed red line) are presented with respect to  $\Delta$  keeping a fixed  $\mu = 2.0$ . This is a representative case, we observe similar nature for various other system-sizes as well. The finite-size scaling of  $\mathcal{F}_{\Delta\Delta}$  and  $\mathcal{G}$  are presented in (b) and (c), respectively. Setting  $\mu = 2$ ,  $\mathcal{F}_{\Delta\Delta}$  and  $\mathcal{G}$  at  $\Delta = 10^{-7}$  (circular markers) scale as  $\mathcal{F}_{\Delta\Delta}^a \sim L^2$  and  $\mathcal{G}^a \sim L^6$ , while at  $\Delta = 0.7$  (square markers) they scale as  $\mathcal{F}_{\Delta\Delta}^b \sim L$  and  $\mathcal{G}^b \sim L$ . The straight lines are the best fit. (d) We present the scaling exponents  $\beta$  of  $\mathcal{F}_{\Delta\Delta}$  and  $\mathcal{G}$  against the parameter  $\Delta$ . We identify three regions, (i) low  $\Delta$  regime:  $\Delta < 10^{-5}$  is represented by light blue color where  $\mathcal{F}_{\Delta\Delta} \sim L^2$  and  $\mathcal{G} \sim L^6$ ; (ii) intermediate  $\Delta$  regime:  $10^{-5} \leq \Delta \leq 0.03$  represented by light green color where  $\beta$  transitions for both  $\mathcal{F}_{\Delta\Delta}$  and  $\mathcal{G}$ ; (iii) large  $\Delta$  regime:  $\Delta > 0.03$  is represented by light pink color where  $\mathcal{F}_{\Delta\Delta}, \mathcal{G} \sim L$ . The parameter  $\mu = 2$  is fixed throughout.

obtain closed form expressions of the leading order scalings as,  $\mathcal{F}_{\mu\mu} \sim \Delta^2 L^6 / \pi^6$ ,  $\mathcal{F}_{\Delta\Delta} \sim L^2 / 8$ ,  $\mathcal{F}_{\mu\Delta} \sim \Delta L^4 / \pi^4$  and  $\mathcal{G} \sim (\pi^2 - 8) \Delta^2 L^6 / \pi^8$ . Thus, we observe super-Heisenberg scaling in all quantities of our interest except  $\mathcal{F}_{\Delta\Delta}$  for which it saturates the Heisenberg limit. These scalings of the QFIM are remarkable results establishing the importance of the multicritical point and symmetry-breaking for precision measurement of multiple parameters. This constitutes the main result of our work. The details of the derivations for obtaining the analytical expressions are presented in Appendix B.

*$\mathcal{F}_{\mu\mu}$  at multicriticality and beyond.*— As mentioned before,  $\mathcal{F}_{\mu\mu} = \sum_k \frac{\Delta^2 \sin^2 k}{\mathcal{E}_k^4}$ . Evidently,  $\mathcal{F}_{\mu\mu}$  vanishes on the critical line,  $\Delta = 0$ . A non-vanishing value  $\mathcal{F}_{\mu\mu}$  requires to prepare the system at a finite  $\Delta$ . In Fig. 2(a), we show the nature of  $\mathcal{F}_{\mu\mu}$  with respect to  $\mu$ , for a representative case, where  $\Delta$  is set at  $0.001$ .  $\mathcal{F}_{\mu\mu}$  develops a peak at  $\mu \sim 2.0$ . The peak corresponds to a gap-to-gapless transition. In Fig. 2(b), we present the finite-size scaling of  $\mathcal{F}_{\mu\mu}$  at  $\mu = 2$  and for two representative cases of  $\Delta = 10^{-7}$  with scaling exponent  $\beta = 6$  and  $\Delta = 0.7$  with  $\beta = 1$ . This change in scaling exponent is gradual with change in the value of  $\Delta$  and is presented in Fig. 2(c). We observe that based on the value of

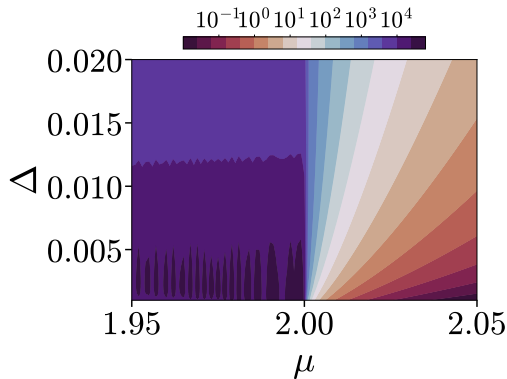


FIG. 4. **Variation of  $\mathcal{G}$  near multicriticality** : The quantity  $\mathcal{G}$  is presented with respect to the tuning parameters  $\mu$  and  $\Delta$  in the vicinity of the multicriticality. The probe considered is the ground state of the Kitaev model on a one-dimensional lattice with system size of  $L = 1000$ .

$\beta$ , the parameter range of  $\Delta$  can be divided into three parts: small  $\Delta$ -regime with super-Heisenberg  $\beta = 6$ , intermediate  $\Delta$ -regime where the  $\beta$  transitions from super-HL to SQL and large  $\Delta$ -regime where we observe SQL scaling, i.e.,  $\beta = 1$ .

*$\mathcal{F}_{\Delta\Delta}$  and  $\mathcal{G}$  at multicriticality and beyond.*— Following expressions are obtained:  $\mathcal{F}_{\Delta\Delta} = \sum_k \frac{z_k^2 \sin^2 k}{\mathcal{E}_k^4}$  and  $\mathcal{F}_{\mu\Delta} = \sum_k \frac{\Delta z_k \sin^2 k}{\mathcal{E}_k^4}$ .  $\mathcal{G}$  can be computed from there-off as it is a function of  $\mathcal{F}_{ab}$ , where  $a, b = \mu, \Delta$ . Validity of these expressions are further confirmed numerically. It is, however, imperative that while changing both the parameters simultaneously in an adiabatic manner, it is done in such a fashion that the parameter  $\mu$  does not follow the critical  $\Delta = 0$ , along which  $\mathcal{F}_{\mu\Delta}$  vanishes. Hence, the variation in  $\mu$  must be guided entirely within the symmetry-broken phase with non-vanishing  $\Delta$ , and such that it encounter a gap-to-gapless transition. The parameter  $\Delta$ , however, can be navigated along the critical line,  $\mu = 2$ , such that it involves the symmetry-breaking transition. The combined effects of the gap-to-gapless transition and the symmetry-breaking gives rise to a super-Heisenberg scaling, as we exemplify below. It is by now obvious that the case of single parameter estimation  $\mathcal{F}_{\Delta\Delta}$  can be done solely via symmetry-breaking by tuning  $\mu$  precisely at  $\mu = 2$  and by preparing the system at or near the multicritical point.

We present a set of results displaying the behavior and scaling of  $\mathcal{F}_{\Delta\Delta}$  and  $\mathcal{G}$  with respect to the  $\Delta$  in Fig. 3(a-d). In Fig. 3(a) we present how  $\mathcal{F}_{\Delta\Delta}$  varies with the parameter  $\Delta$  when  $\mu = 2$  for various system-sizes. We observe that  $\mathcal{F}_{\Delta\Delta}$  saturates to a particular maximum value as  $\Delta \rightarrow 0$ . The quantity  $\mathcal{F}_{\Delta\Delta}$  at  $\mu = 2$  becomes independent of  $\Delta$  ( $\mathcal{F}_{\Delta\Delta} \sim L^2/8$ ) for very small values of  $\Delta$ , say up-to  $\Delta^*$ . As the value of  $\Delta$  increases,  $\mathcal{F}_{\Delta\Delta}$  decreases gradually with increase in  $\Delta$ . It can be expected that  $\Delta^* \rightarrow 0$  in the thermodynamic limit. In Fig. 3(b) the finite-size scaling of  $\mathcal{F}_{\Delta\Delta}$  is presented at  $\mu = 2$  for two representative cases,  $\Delta = 10^{-7}$  with super-HL scaling  $\beta = 2$  and  $\Delta = 0.7$  with SQL scaling  $\beta = 1$ . We provide a similar analysis for  $\mathcal{G}$  in Fig. 3(c), where

we show that  $\mathcal{G}$  has super-HL of  $\beta = 6$  at  $\Delta = 10^{-7}$  but a SQL scaling at a larger  $\Delta = 0.7$ . In Fig. 3(d) we provide the change in the scaling exponent of  $\mathcal{F}_{\Delta\Delta}$  and  $\mathcal{G}$  with change in  $\Delta$ . The range of values of  $\Delta$  can be divided into three sub-parts: small  $\Delta$  region where the scaling of  $\mathcal{F}_{\Delta\Delta}$  saturates to HL  $\beta = 2$  as  $\Delta$  decreases and  $\mathcal{G}$  has a super-HL scaling of 6. In the intermediate  $\Delta$  range the scaling exponents of both of the quantities transition to SQL value of  $\beta = 1$ . In the large  $\Delta$  region the scaling exponents of both the quantities saturate to 1.

In Fig. 4, we present the variation of  $\mathcal{G}$  with respect to the parameters  $\mu$  and  $\Delta$  for system-size  $L = 1000$ . This is a representative case, and we observe similar behavior for other system-sizes as well. We observe that the value of  $\mathcal{G}$  is maximum around the critical point of  $\mu = 2.0$ . The nature of  $\mathcal{G}$  is similar to that of  $\mathcal{F}_{\Delta\Delta}$  in the topological regime ( $\mu < 2.0$ ) and is similar to  $\mathcal{F}_{\mu\mu}$  in the trivial phase ( $\mu > 2.0$ ). The scaling exponent  $\beta$  of  $\mathcal{G}$  saturates to 6 for smaller values of  $\Delta$  and saturates to 1 for larger values. The precision limit is inversely proportional to the quantity  $\mathcal{G}$ . Hence, total uncertainty for equally weighted multi-parameter estimation is  $\delta\mu^2 + \delta\Delta^2 \propto \mathcal{G}^{-1} \sim L^{-\beta}$ , where  $\beta$  is the scaling exponent of  $\mathcal{G}$ , viz.  $\mathcal{G} \sim L^\beta$ . Thus, larger the scaling of  $\mathcal{G}$ , the more precisely can one simultaneously sense  $\mu$  and  $\Delta$  for larger system-sizes. Hence, the ground state of the Kitaev model on a one-dimensional lattice, when used as a probe, is a resource for obtaining quantum-enhanced multi-parameter sensitivity.

#### IV. DISCUSSIONS

There has been several proposals for engineering many-body quantum sensors by exploiting criticality. In all these works reported so far, gap-to-gapless transition has been identified as the key resource for achieving the quantum enhanced sensing. Other important concept associated with quantum criticality, such as symmetry-breaking, has not been shown so far to play any crucial role in parameter estimation. In this work we demonstrate for the first time that symmetry-breaking can also be a useful resource in parameter estimation. We show this by exploiting the the ground-state of the Kitaev model on a one-dimensional lattice as a candidate for a multi-parameter sensor.

The probe acting as an adiabatic sensor provides quantum-enhanced sensitivity near the multicritical point. The system admits a topological phase for  $|\mu| \leq 2$  and a trivial phase beyond that. The topological phase is characterized by a non-zero winding number. In addition, the  $\Delta = 0$  point brings about a flip in the sign of the winding number when the system is in the topological phase. At the critical point of  $\mu = 2.0$  and  $\Delta = 10^{-7}$ , we obtain single-parameter scaling of the QFI-s  $\mathcal{F}_{\mu\mu} \sim L^6$  and  $\mathcal{F}_{\Delta\Delta} \sim L^2$ , whereas the multi-parameter sensitivity at this point also touches  $\mathcal{G} \sim L^6$  mark. Beyond this point, we do get quantum advantage in the form of super-SQL scaling for an extended region of the parameter-space. In our work, we present a phase diagram of the system and discuss how the QFIM and total uncertainty limit behave in the parameter-space of either side of the critical line.



In summary, thus, it can be said that the symmetry-breaking transition can be used as a resource, similar to gap-gapless transition, for engineering a new class of quantum sensors, as demonstrated by considering the topological Kitaev chain. It will be interesting to pursue further investigations in future, such as understanding the effects of long-range tunneling or long-range pairing on the sensing protocols proposed in this work.

### Appendix A: Theory of multi-parameter Sensing

Let us consider a set of parameters,  $\mathbf{x} = \{x_a\}_{a=1}^n$ , encoded in some density matrix  $\rho(\mathbf{x})$ . The precision limits of any parameter that is being sensed is given by a  $n \times n$  matrix called the Quantum Fisher Information Matrix (QFIM). The elements of the QFIM represented by  $\mathcal{F}$  is given by,  $\mathcal{F}_{ab} := \frac{1}{2}\text{Tr}(\rho\{L_a, L_b\})$ , where  $\{\cdot, \cdot\}$  represents the anti-commutation and the operators  $L_a$  and  $L_b$  are the symmetric logarithmic derivatives (SLD) with respect to  $x_a$  and  $x_b$ , respectively. This is given by the equation,  $\partial_i \rho = \frac{1}{2}(\rho L_i + L_i \rho)$ , where,  $i = a, b$  and  $\partial_i$  is the partial derivative with respect to  $x_i$  viz.  $\partial_i = \partial/\partial x_i$ . In this work, we specifically work with the many-body ground state of the Kitaev model as described in the previous section. Hence our state of interest is a pure state. For pure states, the entry  $\mathcal{F}_{ab}$  reduces to  $\mathcal{F}_{ab} = 4\text{Re}(\langle \partial_a \psi | \partial_b \psi \rangle - \langle \partial_a \psi | \psi \rangle \langle \psi | \partial_b \psi \rangle)$ . Here the state  $|\psi\rangle = |\psi(\mathbf{x})\rangle$  encodes the parameters  $\mathbf{x}$ . It can be seen that the diagonal elements of QFIM -  $\mathcal{F}_{aa}$  reduces to the quantum fisher information for parameter  $x_a$ .

The parameters  $\mu, \Delta$  of the hamiltonian in Eq. (1) are encoded in the ground state. The adiabatic changes in these parameters gets reflected in the ground state. By employing the methods of the QFIM, we get a  $2 \times 2$  matrix  $\mathcal{F}$ , given by

$$\mathcal{F} = \begin{pmatrix} \mathcal{F}_{\mu\mu} & \mathcal{F}_{\mu\Delta} \\ \mathcal{F}_{\Delta\mu} & \mathcal{F}_{\Delta\Delta} \end{pmatrix}. \quad (\text{A1})$$

The precision limit of a multi-parameter estimation is quantified using the covariance matrix,  $\text{Cov}(\mathbf{x})$ . This is given by

$$\text{Cov}_{ij}(\mathbf{x}) := \langle x_i x_j \rangle - \langle x_i \rangle \langle x_j \rangle. \quad (\text{A2})$$

The QFIM  $\mathcal{F}$  is related to the covariance matrix  $\text{Cov}(\mu, \Delta)$  and obeys following Cramér-Rao inequality:

$$\text{Cov}(\mu, \Delta) \geq \frac{1}{m} \mathcal{F}^{-1}(\mu, \Delta). \quad (\text{A3})$$

Taking trace on both sides of the matrix inequality one obtains the scalar inequality,

$$\delta\mu^2 + \delta\Delta^2 \geq \frac{1}{m} \frac{\mathcal{F}_{\mu\mu} + \mathcal{F}_{\Delta\Delta}}{\mathcal{F}_{\mu\mu}\mathcal{F}_{\Delta\Delta} - \mathcal{F}_{\Delta\mu}\mathcal{F}_{\mu\Delta}} = \frac{1}{m} \mathcal{G}^{-1}, \quad (\text{A4})$$

where we define,

$$\mathcal{G} := (\text{Tr}[\mathcal{F}^{-1}])^{-1} = \frac{\mathcal{F}_{\mu\mu}\mathcal{F}_{\Delta\Delta} - \mathcal{F}_{\Delta\mu}\mathcal{F}_{\mu\Delta}}{\mathcal{F}_{\mu\mu} + \mathcal{F}_{\Delta\Delta}}. \quad (\text{A5})$$

The quantity  $\mathcal{G}^{-1}$  is the total uncertainty for the equally weighted multi-parameter estimation and  $m$  is the number of repetition of the sensing protocol. For single-parameter estimation, where both parameters are sensed individually and independently, this precision bound reduces to,

$$\delta\mu^2 + \delta\Delta^2 \geq \frac{1}{m} \left( \frac{1}{\mathcal{F}_{\mu\mu}} + \frac{1}{\mathcal{F}_{\Delta\Delta}} \right). \quad (\text{A6})$$

Note that the off-diagonal terms are symmetric under interchange of  $\mu$  and  $\Delta$ , i.e.,  $\mathcal{F}_{\Delta\mu} = \mathcal{F}_{\mu\Delta}$ . This implies that right-hand side quantity in Eq. (A4) is smaller than that in Eq. (A6), and hence thereby making the Eq. (A4) a tighter bound than the Eq. (A6). Thus, we observe that multi-parameter estimation admits same uncertainty as separate single-parameter estimations, if and only if the parameters under study are uncorrelated.

### Appendix B: Derivation of $\mathcal{F}_{ab}$ for ABC

The elements of QFIM for a pure state are given by,

$$\mathcal{F}_{ab} = 4\text{Re}(\langle \partial_a \psi | \partial_b \psi \rangle - \langle \partial_a \psi | \psi \rangle \langle \psi | \partial_b \psi \rangle). \quad (\text{B1})$$

For the Kitaev model the ground state is of the form [48]:

$$|\Psi_G\rangle = \prod_{k=1}^{L/2} \gamma_k^\dagger |0\rangle, \quad (\text{B2})$$

where  $k$  stands for the momentum states,  $k = (2i-1)\pi/L$ , for  $i = 1, \dots, L/2$ . For brevity, we mark  $k$  via  $i$  in the product above and  $\gamma_k^\dagger = u_k + v_k c_k^\dagger c_{-k}^\dagger$ . Furthermore,

$$u_k = \frac{\mathcal{E}_k + z_k}{\sqrt{2\mathcal{E}_k(\mathcal{E}_k + z_k)}}, \quad v_k = \frac{iy_k}{\sqrt{2\mathcal{E}_k(\mathcal{E}_k + z_k)}}. \quad (\text{B3})$$

Here  $\mathcal{E}_k = 2\sqrt{(\cos k + \frac{\mu}{2})^2 + \frac{1}{4}\Delta^2 \sin^2 k}$ ,  $y_k = -\Delta \sin k$  and  $z_k = -\mu - 2 \cos k$ . Using the form,

$$|\partial_a \Psi_G\rangle = \sum_{k=1}^{L/2} \gamma_1^\dagger \dots (\partial_a u_k + \partial_a v_k c_k^\dagger c_{-k}^\dagger) \dots \gamma_{L/2}^\dagger |0\rangle. \quad (\text{B4})$$

$$\begin{aligned} \Rightarrow \langle \partial_a \Psi_G | \partial_b \Psi_G \rangle &= \sum_{k=1}^{L/2} \partial_a u_k^* \partial_b u_k + \partial_a v_k^* \partial_b v_k. \\ \Rightarrow \langle \partial_a \Psi_G | \Psi_G \rangle &= \sum_{k=1}^{L/2} \partial_a u_k^* u_k + \partial_a v_k^* v_k. \end{aligned} \quad (\text{B5})$$

Using this form, we arrive at the final expression:

$$\begin{aligned} \mathcal{F}_{ab} &= 4 \sum_{k=1}^{L/2} \text{Re} [\partial_a u_k^* \partial_b u_k + \partial_a v_k^* \partial_b v_k] \\ &+ 4\text{Re} \left[ \left( \sum_{k=1}^{L/2} \partial_a u_k^* u_k + \partial_a v_k^* v_k \right) \left( \sum_{k=1}^{L/2} u_k^* \partial_b u_k + v_k^* \partial_b v_k \right) \right]. \end{aligned} \quad (\text{B6})$$

We note that  $\sum_{k=1}^{L/2} \partial_a u_k^* u_k + \partial_a v_k^* v_k = 0$  using  $|u_k|^2 + |v_k|^2 = 1$ . Thus, we get:

$$\mathcal{F}_{ab} = 4 \sum_{k=1}^{L/2} \text{Re} [\partial_a u_k^* \partial_b u_k + \partial_a v_k^* \partial_b v_k]. \quad (\text{B7})$$

We find that:

$$\begin{aligned} \partial_\mu u_k &= \frac{(-\mathcal{E}_k + z_k) \sqrt{\mathcal{E}_k(\mathcal{E}_k + z_k)}}{2\sqrt{2}\mathcal{E}_k^3}, \\ \partial_\mu v_k &= \frac{iy_k \sqrt{\mathcal{E}_k(\mathcal{E}_k + z_k)}}{2\sqrt{2}\mathcal{E}_k^3}, \\ \partial_\Delta u_k &= \frac{-y_k^2 z_k}{2\sqrt{2}\Delta e_k^{5/2} \sqrt{\mathcal{E}_k + z_k}}, \\ \partial_\Delta v_k &= \frac{iy_k z_k (\mathcal{E}_k + z_k)}{2\sqrt{2}\Delta e_k^{5/2} \sqrt{\mathcal{E}_k + z_k}}. \end{aligned} \quad (\text{B8})$$

Subsequently, we get,

$$\begin{aligned} \mathcal{F}_{\mu\mu} &= \sum_k \frac{\Delta^2 \sin^2 k}{\mathcal{E}_k^4}, \\ \mathcal{F}_{\mu\Delta} &= \sum_k \frac{\Delta z_k \sin^2 k}{\mathcal{E}_k^4}, \\ \mathcal{F}_{\Delta\Delta} &= \sum_k \frac{z_k^2 \sin^2 k}{\mathcal{E}_k^4}, \end{aligned} \quad (\text{B9})$$

where  $k = (2i - 1)\pi/L$  and sum is over the values  $i = 1, 2, \dots, L/2$ .

Let's find out the scaling exponents, when we set both  $\Delta \rightarrow 0$  and  $\mu \rightarrow 2$ . We have

$$\begin{aligned} \mathcal{F}_{\mu\mu} &= \sum_k \frac{\Delta^2 \sin^2 k}{(4(\cos k + \frac{\mu}{2})^2 + \Delta^2 \sin^2 k)^2}, \\ &\approx \sum_k \frac{\Delta^2 \sin^2 k}{16(\cos k + 1)^4} + \mathcal{O}(\Delta^4). \end{aligned} \quad (\text{B10})$$

Now, as we can see the numerator tends to zero. Therefore, largest contribution of this sum comes from the terms where the denominator also tends to zero, i.e.,  $k \rightarrow \pi$ . This is achieved by the last term in the sum, which is given by setting  $i = L/2$  and therefore  $k = \pi - \pi/L$ . We thus get,

$$\mathcal{F}_{\mu\mu} \approx \frac{\Delta^2 \sin^2(\pi - \frac{\pi}{L})}{16(\cos(\pi - \frac{\pi}{L}) + 1)^4} - \frac{\Delta^4 \sin^4(\pi - \frac{\pi}{L})}{64(\cos(\pi - \frac{\pi}{L}) + 1)^6}. \quad (\text{B11})$$

In the limit of large  $L$ , we get

$$\mathcal{F}_{\mu\mu} \approx \frac{\Delta^2 L^6}{\pi^6} + \mathcal{O}(\Delta^4). \quad (\text{B12})$$

Thus, we have  $\mathcal{F}_{\mu\mu} \sim L^6$  for  $\Delta \rightarrow 0$  and  $\mu \rightarrow 2$ . Using similar arguments it can be easily shown that  $\mathcal{F}_{\mu\mu} \sim L^2$ , when  $\mu \rightarrow 2$  and  $|\Delta| \gg 0$ .

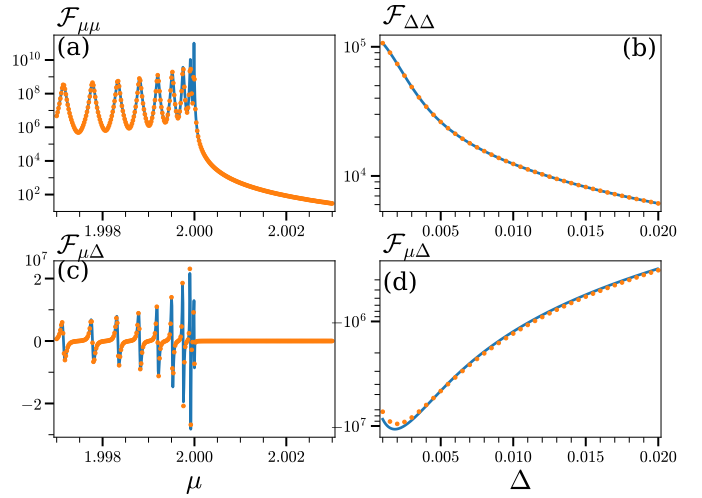


FIG. B.1. **Comparison between analytic expression (B9) of the QFIM and their corresponding values obtained numerically:** The elements of QFIM are presented with change in  $\mu$  or  $\Delta$ , i.e., (a)  $\mathcal{F}_{\mu\mu}$  against  $\mu$ , (b)  $\mathcal{F}_{\Delta\Delta}$  against  $\Delta$ , (c)  $\mathcal{F}_{\mu\Delta}$  against  $\mu$  and (d)  $\mathcal{F}_{\mu\Delta}$  against  $\Delta$ . This is a representative case of system-size  $L = 1000$ , where  $\Delta = 0.001$  in (a) and (c), while  $\mu = 2.0$  in (b) and (d). The blue lines are obtained from the Eq.(B9), while the orange circular markers are obtained numerically for the Kitaev chain with anti-periodic boundary condition. The y-axes of (a),(b) and (d) are in log-scale while the y-axis of (c) is in linear-scale. The x-axes of all four are in linear-scale.

For  $\mathcal{F}_{\Delta\Delta}$  in the limit  $\Delta \rightarrow 0$  and  $\mu \rightarrow 2$ , we have

$$\mathcal{F}_{\Delta\Delta} \approx \sum_k \frac{1}{4} \tan^2 \left( \frac{k}{2} \right) + \mathcal{O}(\Delta^2). \quad (\text{B13})$$

We observe that the larger values of  $k$  dominate this sum. By considering the contributions to the sum in descending order of the  $k = \pi - \frac{\pi}{L}$ , one finds

$$\begin{aligned} \mathcal{F}_{\Delta\Delta} &\approx \frac{1}{4} \tan^2 \left( \frac{\pi}{2} - \frac{\pi}{2L} \right) + \frac{1}{4} \tan^2 \left( \frac{\pi}{2} - \frac{3\pi}{2L} \right) + \dots \\ &= \frac{1}{4} \cot^2 \left( \frac{\pi}{2L} \right) + \frac{1}{4} \cot^2 \left( \frac{3\pi}{2L} \right) + \dots \\ &\approx \frac{L^2}{\pi^2} \left( 1 + \frac{1}{9} + \frac{1}{25} \dots + \frac{1}{m^2} \right). \end{aligned} \quad (\text{B14})$$

Here, we terminate the series at some  $m \ll L/2$ . Now we note that the Riemann zeta function at  $n = 2$  is given by

$$\begin{aligned} \zeta(2) &= \sum_{n=1}^{\infty} \frac{1}{n^2} = \sum_k = \frac{\pi^2}{6}, \\ &\Rightarrow \left( 1 + \frac{1}{9} + \frac{1}{25} + \dots \right) = \frac{3}{4} \zeta(2) = \frac{\pi^2}{8}. \end{aligned} \quad (\text{B15})$$

For very large  $L$  and consequently large  $m$ , we can approximate the sum in bracket of (B14) with (B15). We thus get,

$$\mathcal{F}_{\Delta\Delta} \approx \frac{L^2}{8} + \mathcal{O}(\Delta^2). \quad (\text{B16})$$

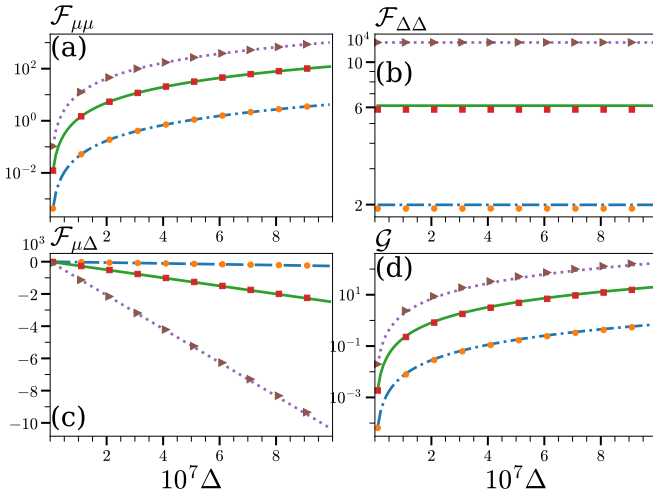


FIG. B.2. *Comparison between (B9) and (B19)*: The analytic form of the elements of the Quantum Fisher Information matrix: (a)  $\mathcal{F}_{\mu\mu}$ , (b)  $\mathcal{F}_{\Delta\Delta}$ , (c)  $\mathcal{F}_{\mu\Delta}$  and (d)  $\mathcal{G}$  are presented with respect to  $\Delta$  which is in the range  $\Delta \in [10^{-8}, 10^{-6}]$ , keeping a fixed  $\mu = 2$ . We numerically confirm that these quantities (B9) and its approximations (B19) in the small  $\Delta$  regime matches. The markers indicate the approximated functions (B19) and the lines correspond to (B9). These are plotted for system sizes  $L = 400$  (circular markers, dot-dashed line),  $700$  (square markers, solid line) and  $1000$  (triangular markers, dotted line). The markers and line-styles are uniform across all the four sub-figures. The y-axes are in log-scale in (a),(b) and (d) and in linear-scale in (c). The x-axis is in linear-scale and the labels are multiplied by  $10^7$  for convenience.

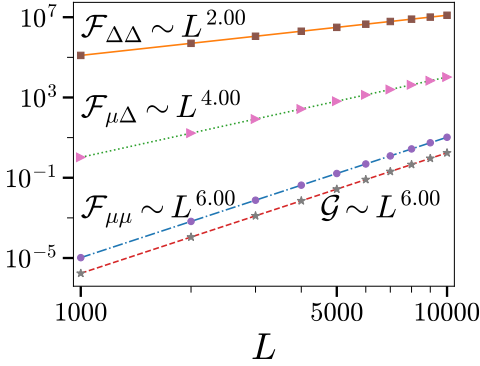


FIG. B.3. *Finite-size scaling of elements QFIM and  $\mathcal{G}$* : We evaluate  $\mathcal{F}_{\mu\mu}$  (circular markers),  $\mathcal{F}_{\Delta\Delta}$  (square markers),  $-\mathcal{F}_{\mu\Delta}$  (triangular markers) and  $\mathcal{G}$  (star markers) at the point  $\Delta = 10^{-10}$  and  $\mu = 2.0$  using Eq.(B9) for system-sizes from  $L = 1000$  to  $10000$ . The scaling exponents match with the ones obtained in Eq.(B19). The lines represent the best fits.

Hence, we have  $\mathcal{F}_{\Delta\Delta} \sim L^2$  for  $\Delta \rightarrow 0$  and  $\mu \rightarrow 2$ . Following a similar line of reasoning as Eq.(B11), we get

$$\mathcal{F}_{\mu\Delta} \approx -\frac{\Delta L^4}{\pi^4} + \mathcal{O}(\Delta^3). \quad (\text{B17})$$

Thus, we have  $-\mathcal{F}_{\mu\Delta} \sim L^4$  for  $\Delta \rightarrow 0$  and  $\mu \rightarrow 2$ . Now,

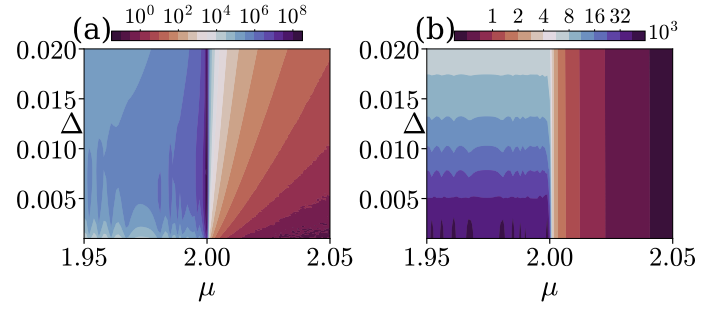


FIG. B.4. *Elements of the Quantum Fisher Information matrix*: The QFIM elements (a)  $\mathcal{F}_{\mu\mu}$  and (b)  $\mathcal{F}_{\Delta\Delta}$  are presented with respect to the tuning parameters  $\mu$  and  $\Delta$  in the vicinity of the critical points of either axes. The probe considered is the ground state of the Kitaev model on a one-dimensional lattice with system size of  $L = 1000$ . Note that in (b) the Fisher information is in the range of  $10^3$ . In both figures, the elements of QFIM are presented in log-scale.

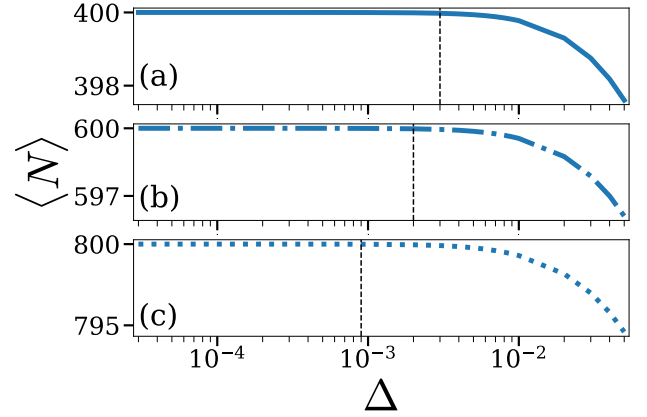


FIG. B.5. *Change in the average particle number  $\langle N \rangle$  with change in  $\Delta$* : The average particle number of the probe state (B2) is numerically obtained and is presented with a fixed  $\mu = 2$  throughout. This a representative case for three system sizes : (a)  $L = 400$  (dot-dashed line), (b)  $L = 600$  (solid line) and (c)  $L = 800$  (dotted line).

for the case of  $\mathcal{G}$ , it can be shown that

$$\mathcal{G} \approx \frac{(\pi^2 - 8)\Delta^2}{\pi^8} L^6 + \mathcal{O}(\Delta^4). \quad (\text{B18})$$

Thus, we have  $\mathcal{G} \sim L^6$  for  $\Delta \rightarrow 0$  and  $\mu \rightarrow 2$ . In summary, one obtains,

$$\begin{aligned} \mathcal{F}_{\mu\mu} &\approx \frac{\Delta^2}{\pi^6} L^6, \\ \mathcal{F}_{\Delta\Delta} &\approx \frac{1}{8} L^2, \\ \mathcal{F}_{\mu\Delta} &\approx -\frac{\Delta}{\pi^4} L^4, \\ \mathcal{G} &\approx \frac{(\pi^2 - 8)\Delta^2}{\pi^8} L^6. \end{aligned} \quad (\text{B19})$$

In Fig. B.4 we present (a)  $\mathcal{F}_{\mu\mu}$  and (b)  $\mathcal{F}_{\Delta\Delta}$  for system-size  $L = 1000$ . We observe a similar nature for other system-sizes as well. Figure B.4 quite clearly shows the transition

from topological to trivial phase at  $\mu = 2.0$ . We see in Fig. B.4(a) that the system achieves its maximum  $\mathcal{F}_{\mu\mu}$  at the point  $\mu = 2.0$ . The quantity  $\mathcal{F}_{\mu\mu}$  gradually decreases as we move further into the trivial phase. Due to the apparent fluctuations of  $\mathcal{F}_{\mu\mu}$  in the topological phase of the finite-sized systems, particularly in smaller systems, numerical calculations were not pushed in the smaller  $\Delta$  regime. We, however, performed the scaling analysis in the trivial phase away from the critical line. In Fig. B.4(b), we present the component  $\mathcal{F}_{\Delta\Delta}$  of QFIM. The figure clearly shows that this quantity increases as we move nearer to  $\Delta = 0$  line, across which the system the topological invariant undergoes a discrete jump, i.e., a flip in sign of the winding number, given  $|\mu| \leq 2$ .

In Fig. B.5, we present the average particle number  $\langle N \rangle$  of the probe state, i.e., the ground state of the Kitaev model in one dimension for  $\mu = 2$ . As seen from the Hamiltonian of the Kitaev model, the  $p$ -wave superconductivity term with coupling  $\Delta$  makes the system particle-number non-conserving. This means that when  $\Delta$  is set to a non-zero value, the ground state wave-function becomes a superposition of various particle-number sector. When  $\Delta$  is set to zero, we note two things: the states with fixed momentum become eigenstates of the Hamiltonian and the value of  $\mu$  determines the fixed particle-number sector to which the ground state be-

longs to. We note that at  $\mu = 0$  limit, half of the single-particle states have negative eigenenergies. The many-body ground state of the model is constructed by filling the negative energy states via fermions. Since there is a negative sign with  $\mu$  in the Hamiltonian, more single-particle eigenstates with negative energies becomes available with increasing  $\mu$ . Thus, occupation number of the ground state increases gradually with increasing  $\mu$ . On introducing a non-zero  $\Delta$ , the ground state no longer has a fixed number of particles, rather it is a superposition of many fixed particle-number states. We observe that at very small values of  $\Delta$ , the ground state has the fully-filled state with almost unit probability because of a small  $\Delta$  and a very large  $\mu$ . As the value of  $\Delta$  increases, it becomes energetically more costly to fill up particles than that for smaller  $\Delta$ . Due to this, the average particle-number decreases with increase of  $\Delta$ . Hence, physically it turns out that at the gapless multicritical point ( $\mu = 2$  and  $\Delta = 0$ ), the system is in a trivial band-insulating phase, as all available energy states are filled-up by the fermions. A sufficiently small value of the symmetry-breaking term  $\Delta$ , i.e.,  $\Delta^*$ , ensures the system's transition to a critical  $p$ -wave superconducting phase. This, in turn, facilitates the quantum enhanced sensing despite the fact that adiabatic variation of the parameter,  $\Delta$ , follows the gapless line throughout.

- 
- [1] S. L. Braunstein and C. M. Caves, Statistical distance and the geometry of quantum states, *Phys. Rev. Lett.* **72**, 3439 (1994).
- [2] C. L. Degen, F. Reinhard, and P. Cappellaro, Quantum sensing, *Rev. Mod. Phys.* **89**, 035002 (2017).
- [3] H. Cramér, *Mathematical Methods of Statistics (PMS-9), Volume 9* (Princeton University Press, Princeton, 1946).
- [4] C. W. Helstrom, Quantum detection and estimation theory, *Journal of Statistical Physics* **1**, 231 (1969).
- [5] V. Giovannetti, S. Lloyd, and L. Maccone, Quantum-enhanced measurements: beating the standard quantum limit, *Science* **306**, 1330 (2004).
- [6] V. Giovannetti, S. Lloyd, and L. Maccone, Advances in quantum metrology, *Nature photonics* **5**, 222 (2011).
- [7] H.-L. Shi, X.-W. Guan, and J. Yang, Universal shot-noise limit for quantum metrology with local hamiltonians, *Phys. Rev. Lett.* **132**, 100803 (2024).
- [8] V. Giovannetti, S. Lloyd, and L. Maccone, Quantum metrology, *Phys. Rev. Lett.* **96**, 010401 (2006).
- [9] H. Manshour, M. Zarei, M. Abdi, S. Bose, and A. Bayat, Quantum enhanced sensitivity through many-body bloch oscillations, arXiv preprint arXiv:2406.13921 (2024).
- [10] C. Mukhopadhyay and A. Bayat, Modular many-body quantum sensors, arXiv preprint arXiv:2311.18319 (2023).
- [11] A. Bhattacharyya, D. Saha, and U. Sen, Even-body interactions favour asymmetry as a resource in metrological precision, arXiv preprint arXiv:2401.06729 (2024).
- [12] R. Yousefjani, K. Sacha, and A. Bayat, Discrete time crystal phase as a resource for quantum enhanced sensing, arXiv preprint arXiv:2405.00328 (2024).
- [13] P. Zanardi and N. Paunković, Ground state overlap and quantum phase transitions, *Phys. Rev. E* **74**, 031123 (2006).
- [14] S.-J. Gu, H.-M. Kwok, W.-Q. Ning, and H.-Q. Lin, Fidelity susceptibility, scaling, and universality in quantum critical phenomena, *Phys. Rev. B* **77**, 245109 (2008).
- [15] P. Zanardi, M. G. A. Paris, and L. Campos Venuti, Quantum criticality as a resource for quantum estimation, *Phys. Rev. A* **78**, 042105 (2008).
- [16] C. Invernizzi, M. Korbman, L. Campos Venuti, and M. G. A. Paris, Optimal quantum estimation in spin systems at criticality, *Phys. Rev. A* **78**, 042106 (2008).
- [17] S.-J. GU, Fidelity approach to quantum phase transitions, *International Journal of Modern Physics B* **24**, 4371 (2010), <https://doi.org/10.1142/S0217979210056335>.
- [18] S. Gammelmark and K. Mølmer, Phase transitions and heisenberg limited metrology in an ising chain interacting with a single-mode cavity field, *New Journal of Physics* **13**, 053035 (2011).
- [19] M. Skotiniotis, P. Sekatski, and W. Dür, Quantum metrology for the ising hamiltonian with transverse magnetic field, *New Journal of Physics* **17**, 073032 (2015).
- [20] M. M. Rams, P. Sierant, O. Dutta, P. Horodecki, and J. Zakrzewski, At the limits of criticality-based quantum metrology: Apparent super-heisenberg scaling revisited, *Phys. Rev. X* **8**, 021022 (2018).
- [21] B.-B. Wei, Fidelity susceptibility in one-dimensional disordered lattice models, *Phys. Rev. A* **99**, 042117 (2019).
- [22] Y. Chu, S. Zhang, B. Yu, and J. Cai, Dynamic framework for criticality-enhanced quantum sensing, *Phys. Rev. Lett.* **126**, 010502 (2021).
- [23] W. J. Huggins, J. R. McClean, N. C. Rubin, Z. Jiang, N. Wiebe, K. B. Whaley, and R. Babbush, Efficient and noise resilient measurements for quantum chemistry on near-term quantum computers, *npj Quantum Information* **7**, 23 (2021).
- [24] S. S. Mirkhalaf, D. Benedicto Orenes, M. W. Mitchell, and E. Witkowska, Criticality-enhanced quantum sensing in ferromagnetic bose-einstein condensates: Role of readout mea-



- surement and detection noise, *Physical Review A* **103**, 023317 (2021).
- [25] R. Di Candia, F. Minganti, K. Petrovniin, G. Paraoanu, and S. Felicetti, Critical parametric quantum sensing, *npj Quantum Information* **9**, 23 (2023).
- [26] R. Salvia, M. Mehboudi, and M. Perarnau-Llobet, Critical quantum metrology assisted by real-time feedback control, *Phys. Rev. Lett.* **130**, 240803 (2023).
- [27] U. Mishra and A. Bayat, Driving enhanced quantum sensing in partially accessible many-body systems, *Phys. Rev. Lett.* **127**, 080504 (2021).
- [28] V. Montenegro, U. Mishra, and A. Bayat, Global sensing and its impact for quantum many-body probes with criticality, *Phys. Rev. Lett.* **126**, 200501 (2021).
- [29] V. Montenegro, G. S. Jones, S. Bose, and A. Bayat, Sequential measurements for quantum-enhanced magnetometry in spin chain probes, *Phys. Rev. Lett.* **129**, 120503 (2022).
- [30] Monika, L. G. C. Lakkaraju, S. Ghosh, and A. S. De, Better sensing with variable-range interactions (2023), [arXiv:2307.06901 \[quant-ph\]](https://arxiv.org/abs/2307.06901).
- [31] S. Singh, L. G. C. Lakkaraju, S. Ghosh, and A. S. De, Dimensional gain in sensing through higher-dimensional quantum spin chain (2024), [arXiv:2401.14853 \[quant-ph\]](https://arxiv.org/abs/2401.14853).
- [32] S. Dooley, S. Pappalardi, and J. Goold, Entanglement enhanced metrology with quantum many-body scars, *Phys. Rev. B* **107**, 035123 (2023).
- [33] V. Montenegro, M. G. Genoni, A. Bayat, and M. G. A. Paris, Quantum metrology with boundary time crystals, *Communications Physics* **6**, 304 (2023).
- [34] L. Pezzè, A. Trenkwalder, and M. Fattori, Adiabatic sensing enhanced by quantum criticality, *arXiv preprint arXiv:1906.01447* (2019).
- [35] X. He, R. Yousefjani, and A. Bayat, Stark localization as a resource for weak-field sensing with super-heisenberg precision, *Phys. Rev. Lett.* **131**, 010801 (2023).
- [36] A. Sahoo, U. Mishra, and D. Rakshit, Localization-driven quantum sensing, *Phys. Rev. A* **109**, L030601 (2024).
- [37] Y.-R. Zhang, Y. Zeng, H. Fan, J. Q. You, and F. Nori, Characterization of topological states via dual multipartite entanglement, *Phys. Rev. Lett.* **120**, 250501 (2018).
- [38] J. Lambert and E. S. Sørensen, Revealing divergent length scales using quantum fisher information in the kitaev honeycomb model, *Phys. Rev. B* **102**, 224401 (2020).
- [39] S. Yin, J. Song, Y. Zhang, and S. Liu, Quantum fisher information in quantum critical systems with topological characterization, *Phys. Rev. B* **100**, 184417 (2019).
- [40] Y.-R. Zhang, Y. Zeng, T. Liu, H. Fan, J. Q. You, and F. Nori, Multipartite entanglement of the topologically ordered state in a perturbed toric code, *Phys. Rev. Res.* **4**, 023144 (2022).
- [41] J. Yang, S. Pang, A. del Campo, and A. N. Jordan, Superheisenberg scaling in hamiltonian parameter estimation in the long-range kitaev chain, *Phys. Rev. Res.* **4**, 013133 (2022).
- [42] S. Sarkar, C. Mukhopadhyay, A. Alase, and A. Bayat, Free-fermionic topological quantum sensors, *Phys. Rev. Lett.* **129**, 090503 (2022).
- [43] J. Wiersig, Enhancing the sensitivity of frequency and energy splitting detection by using exceptional points: Application to microcavity sensors for single-particle detection, *Phys. Rev. Lett.* **112**, 203901 (2014).
- [44] H. Schomerus, Nonreciprocal response theory of non-hermitian mechanical metamaterials: Response phase transition from the skin effect of zero modes, *Phys. Rev. Res.* **2**, 013058 (2020).
- [45] J. C. Budich and E. J. Bergholtz, Non-hermitian topological sensors, *Phys. Rev. Lett.* **125**, 180403 (2020).
- [46] F. Koch and J. C. Budich, Quantum non-hermitian topological sensors, *Phys. Rev. Res.* **4**, 013113 (2022).
- [47] A. Y. Kitaev, Unpaired majorana fermions in quantum wires, *Physics-Uspekhi* **44**, 131 (2001).
- [48] G. B. Mbeng, A. Russomanno, and G. E. Santoro, The quantum Ising chain for beginners, *SciPost Phys. Lect. Notes* , 82 (2024).
- [49] M. Leijnse and K. Flensberg, Introduction to topological superconductivity and majorana fermions, *Semiconductor Science and Technology* **27**, 124003 (2012).
- [50] S. R. Elliott and M. Franz, Colloquium: Majorana fermions in nuclear, particle, and solid-state physics, *Rev. Mod. Phys.* **87**, 137 (2015).
- [51] S. Maity, U. Bhattacharya, and A. K. Dutta, One-dimensional quantum many body systems with long-range interactions, *Journal of Physics A: Mathematical and Theoretical* **53** (2019).
- [52] L. Pezzè, M. Gabbriellini, L. Lepori, and A. Smerzi, Multipartite entanglement in topological quantum phases, *Phys. Rev. Lett.* **119**, 250401 (2017).
- [53] M. Z. Hasan and C. L. Kane, Colloquium: Topological insulators, *Rev. Mod. Phys.* **82**, 3045 (2010).
- [54] J. K. Asbóth, L. Oroszlány, and A. Pályi, A short course on topological insulators, *Lecture notes in physics* **919**, 166 (2016).
- [55] I. C. Fulga, F. Hassler, A. R. Akhmerov, and C. W. J. Beenakker, Scattering formula for the topological quantum number of a disordered multimode wire, *Phys. Rev. B* **83**, 155429 (2011).
- [56] J. D. Sau and S. D. Sarma, Realizing a robust practical majorana chain in a quantum-dot-superconductor linear array, *Nature Communications* **3**, 964 (2012).
- [57] R. M. Lutchyn and M. P. A. Fisher, Interacting topological phases in multiband nanowires, *Phys. Rev. B* **84**, 214528 (2011).
- [58] W. DeGottardi, D. Sen, and S. Vishveshwara, Topological phases, majorana modes and quench dynamics in a spin ladder system, *New Journal of Physics* **13**, 065028 (2011).
- [59] W. DeGottardi, D. Sen, and S. Vishveshwara, Majorana fermions in superconducting 1d systems having periodic, quasiperiodic, and disordered potentials, *Phys. Rev. Lett.* **110**, 146404 (2013).
- [60] M. Thakurathi, A. A. Patel, D. Sen, and A. Dutta, Floquet generation of majorana end modes and topological invariants, *Phys. Rev. B* **88**, 155133 (2013).
- [61] J. Fraxanet, U. Bhattacharya, T. Grass, D. Rakshit, M. Lewenstein, and A. Dauphin, Topological properties of the long-range kitaev chain with aubry-andré-harper modulation, *Phys. Rev. Res.* **3**, 013148 (2021).
- [62] L. Fu and C. L. Kane, Superconducting proximity effect and majorana fermions at the surface of a topological insulator, *Phys. Rev. Lett.* **100**, 096407 (2008).
- [63] V. Mourik, K. Zuo, S. M. Frolov, S. Plissard, E. P. Bakkers, and L. P. Kouwenhoven, Signatures of majorana fermions in hybrid superconductor-semiconductor nanowire devices, *Science* **336**, 1003 (2012).
- [64] M. T. Deng, C. L. Yu, G. Y. Huang, M. Larsson, P. Caroff, and H. Q. Xu, Anomalous zero-bias conductance peak in a nb-insb nanowire-nb hybrid device, *Nano Letters* **12**, 6414 (2012).
- [65] A. Das, Y. Ronen, Y. Most, Y. Oreg, M. Heiblum, and H. Shtrikman, Zero-bias peaks and splitting in an al-inas nanowire topological superconductor as a signature of majorana fermions, *Nature Physics* **8**, 887 (2012).
- [66] I. C. Fulga, A. Haim, A. R. Akhmerov, and Y. Oreg, Adaptive tuning of majorana fermions in a quantum dot chain, *New Journal of Physics* **15**, 045020 (2013).
- [67] S. Nadj-Perge, I. K. Drozdov, J. Li, H. Chen, S. Jeon,

- J. Seo, A. H. MacDonald, B. A. Bernevig, and A. Yazdani, Observation of majorana fermions in ferromagnetic atomic chains on a superconductor, *Science* **346**, 602 (2014), <https://www.science.org/doi/pdf/10.1126/science.1259327>.
- [68] J.-S. Xu, K. Sun, Y.-J. Han, C.-F. Li, J. K. Pachos, and G.-C. Guo, Simulating the exchange of majorana zero modes with a photonic system, *Nature Communications* **7**, 13194 (2016).
- [69] Y. Xing, L. Qi, J. Cao, D.-Y. Wang, C.-H. Bai, W.-X. Cui, H.-F. Wang, A.-D. Zhu, and S. Zhang, Controllable photonic and phononic edge localization via optomechanically induced kitaev phase, *Opt. Express* **26**, 16250 (2018).
- [70] T. Dvir, G. Wang, N. van Loo, C.-X. Liu, G. P. Mazur, A. Bordin, S. L. D. ten Haaf, J.-Y. Wang, D. van Driel, F. Zatelli, X. Li, F. K. Malinowski, S. Gazibegovic, G. Badawy, E. P. A. M. Bakkers, M. Wimmer, and L. P. Kouwenhoven, Realization of a minimal kitaev chain in coupled quantum dots, *Nature* **614**, 445 (2023).
- [71] C.-X. Liu, G. Wang, T. Dvir, and M. Wimmer, Tunable superconducting coupling of quantum dots via andreev bound states in semiconductor-superconductor nanowires, *Phys. Rev. Lett.* **129**, 267701 (2022).
- [72] Y. Zhang, Y.-Q. Ge, and Y. xi Liu, Simulation of kitaev model using one-dimensional chain of superconducting qubits and environmental effect on topological states (2023), [arXiv:2302.03834 \[quant-ph\]](https://arxiv.org/abs/2302.03834).
- [73] G. D. Fresco, B. Spagnolo, D. Valenti, and A. Carollo, Multiparameter quantum critical metrology, *SciPost Phys.* **13**, 077 (2022).
- [74] G. Mihailescu, A. Bayat, S. Campbell, and A. K. Mitchell, Multiparameter critical quantum metrology with impurity probes, *Quantum Science and Technology* **9**, 035033 (2024).
- [75] R. Yousefjani, X. He, A. Carollo, and A. Bayat, Nonlinearity-enhanced quantum sensing in stark probes, *arXiv preprint arXiv:2404.10382* (2024).